Deep-Sea Research II ∎ (∎∎∎∎) ∎∎∎–∎∎∎

Contents lists available at ScienceDirect

Deep-Sea Research II

journal homepage: www.elsevier.com/locate/dsr2

Regular article

Importance of deep mixing and silicic acid in regulating phytoplankton biomass and community in the iron-limited Antarctic Polar Front region in summer

Wee Cheah [a,b,*], Mariana A. Soppa [b], Sonja Wiegmann [b], Sharyn Ossebaar [c], Luis M. Laglera [d], Volker H. Strass [b], Juan Santos-Echeandía [e], Mario Hoppema [b], Dieter Wolf-Gladrow [b], Astrid Bracher [b,f]

[a] Research Center for Environmental Changes, Academia Sinica, Taipei, Taiwan
[b] Alfred-Wegener-Institute Helmholtz Centre for Polar and Marine Research, Bremerhaven, Germany
[c] Royal Netherlands Institute for Sea Research, Texel, The Netherlands
[d] FI-TRACE, Departamento de Química, Universidad de las Islas Baleares, Balearic Islands, Spain
[e] Contamination and Biological Effects, Spanish Institute of Oceanography (IEO), Murcia, Spain
[f] Institute of Environmental Physics, University of Bremen, Bremen, Germany

ARTICLE INFO

Keywords:
Phytoplankton
Photophysiology
Nutrients
Antarctic Polar Front

ABSTRACT

Phytoplankton community structure and their physiological response in the vicinity of the Antarctic Polar Front (APF; 44°S to 53°S, centred at 10°E) were investigated as part of the ANT-XXVIII/3 Eddy-Pump cruise conducted in austral summer 2012. Our results show that under iron-limited (<0.3 μmol m^{-3}) conditions, high total chlorophyll-a (TChl-a) concentrations (>0.6 mg m^{-3}) can be observed at stations with deep mixed layer (>60 m) across the APF. In contrast, light was excessive at stations with shallower mixed layer and phytoplankton were producing higher amounts of photoprotective pigments, diadinoxanthin (DD) and diatoxanthin (DT), at the expense of TChl-a, resulting in higher ratios of (DD+DT)/TChl-a. North of the APF, significantly lower silicic acid ($Si(OH)_4$) concentrations (<2 mmol m^{-3}) lead to the domination of nanophytoplankton consisting mostly of haptophytes, which produced higher ratios of (DD+DT)/TChl-a under relatively low irradiance conditions. The $Si(OH)_4$ replete (>5 mmol m^{-3}) region south of the APF, on the contrary, was dominated by microphytoplankton (diatoms and dinoflagellates) with lower ratios of (DD+DT)/TChl-a, despite having been exposed to higher levels of irradiance. The significant correlation between nanophytoplankton and (DD+DT)/TChl-a indicates that differences in taxon-specific response to light are also influencing TChl-a concentration in the APF during summer. Our results reveal that provided mixing is deep and $Si(OH)_4$ is replete, TChl-a concentrations higher than 0.6 mg m^{-3} are achievable in the iron-limited APF waters during summer.

1. Introduction

The Southern Ocean is of major importance for climate as it is responsible for about 40% of the oceanic uptake of atmospheric carbon dioxide (CO_2; Khatiwala et al., 2009). The extent of CO_2 fluxes in the Southern Ocean varies greatly with space and time (Landschützer et al., 2015), due mainly to ocean circulation and biological pump (Hauck et al., 2013; Morrison et al., 2015). In the region north of the Sub-Antarctic Front (SAF) at around 45°S, Sub-Antarctic Mode Water and Antarctic Intermediate Water formed during deep winter convection are carrying surface dissolved and phytoplankton-fixed CO_2 into the ocean interior, which results in a large uptake of atmospheric CO_2 in this region (Rintoul and Trull, 2001; Sabine et al., 2004; Morrison et al., 2015). In contrast, south of 45°S is a region of net CO_2 release to the atmosphere as a result of upwelling of CO_2-enriched waters (Morrison et al., 2015). Rising CO_2 levels in the atmosphere caused by recent anthropogenic activities have driven more CO_2 uptake in the Southern Ocean, altering the spatial distribution of CO_2 fluxes in the Southern Ocean. In particular, the region between 45°S and 55°S, which used to be a net CO_2 release area is now an area of net CO_2 uptake (Khatiwala et al., 2013).

With nitrate (NO_3) and phosphate (PO_4) concentrations in excess all year round, the Southern Ocean has a great potential for primary production, export of organic material, and uptake of CO_2

* Corresponding author at: Research Center for Environmental Changes, Academia Sinica, Taipei, Taiwan.
E-mail address: weecheah@gate.sinica.edu.tw (W. Cheah).

http://dx.doi.org/10.1016/j.dsr2.2016.05.019
0967-0645/

from the atmosphere. However, limiting factors such as light, iron, silicic acid ($Si(OH)_4$), and grazing (Banse, 1996; Boyd, 2002; Hiscock et al., 2003) hinder the full potential of Southern Ocean's biological pump, creating the largest high nutrient low chlorophyll region (de Baar et al., 2005). In general, the waters north of the APF have typical characteristic of low dissolved iron (DFe), $Si(OH)_4$, chlorophyll-a (Chl-a) concentrations, and they are dominated by haptophytes, especially in areas remote from continental influence (e.g. Banse, 1996; Clementson et al., 2001; Hutchins et al., 2001). Surface waters south of the APF are usually rich in macronutrients (NO_3, PO_4, $Si(OH)_4$) with a phytoplankton community dominated by diatoms (Alderkamp et al., 2010). Recently, several studies have shown that even in offshore waters away from continental influence, concentrations of DFe, $Si(OH)_4$, Chl-a, primary production, and phytoplankton composition can differ within a specific zone in the Southern Ocean (e.g. SAZ) (Bowie et al., 2011; de Salas et al., 2011; Westwood et al., 2011).

The physiological response of phytoplankton to different limiting factors (iron, $Si(OH)_4$, and light) is highly complex and can be multifaceted, especially under co-limitation conditions. In addition to nutrient utilisation, the physiological response of phytoplankton to different limiting factors is also imprinted in the coordination of the light harvesting apparatus and can result in community shifts (Falkowski and La Roche, 1991). For example, under iron-light co-limitation conditions, photosynthesis can be limited by light, but the production of light harvesting protein-complexes (e.g. photosystem II and photosystem I) is constrained by iron availability (Sunda and Huntsman, 1997). In contrast, under low iron high light conditions, photoinhibition or photodamage may occur as iron limitation decreases the synthesis of cytochrome b_6f complexes, an enzyme required in the activation of photoprotective mechanisms (Strzepek and Harrison, 2004; van de Poll et al., 2009). Thus, iron-limited cells are less efficient at coping with an environment with rapid irradiance fluctuations than iron-replete

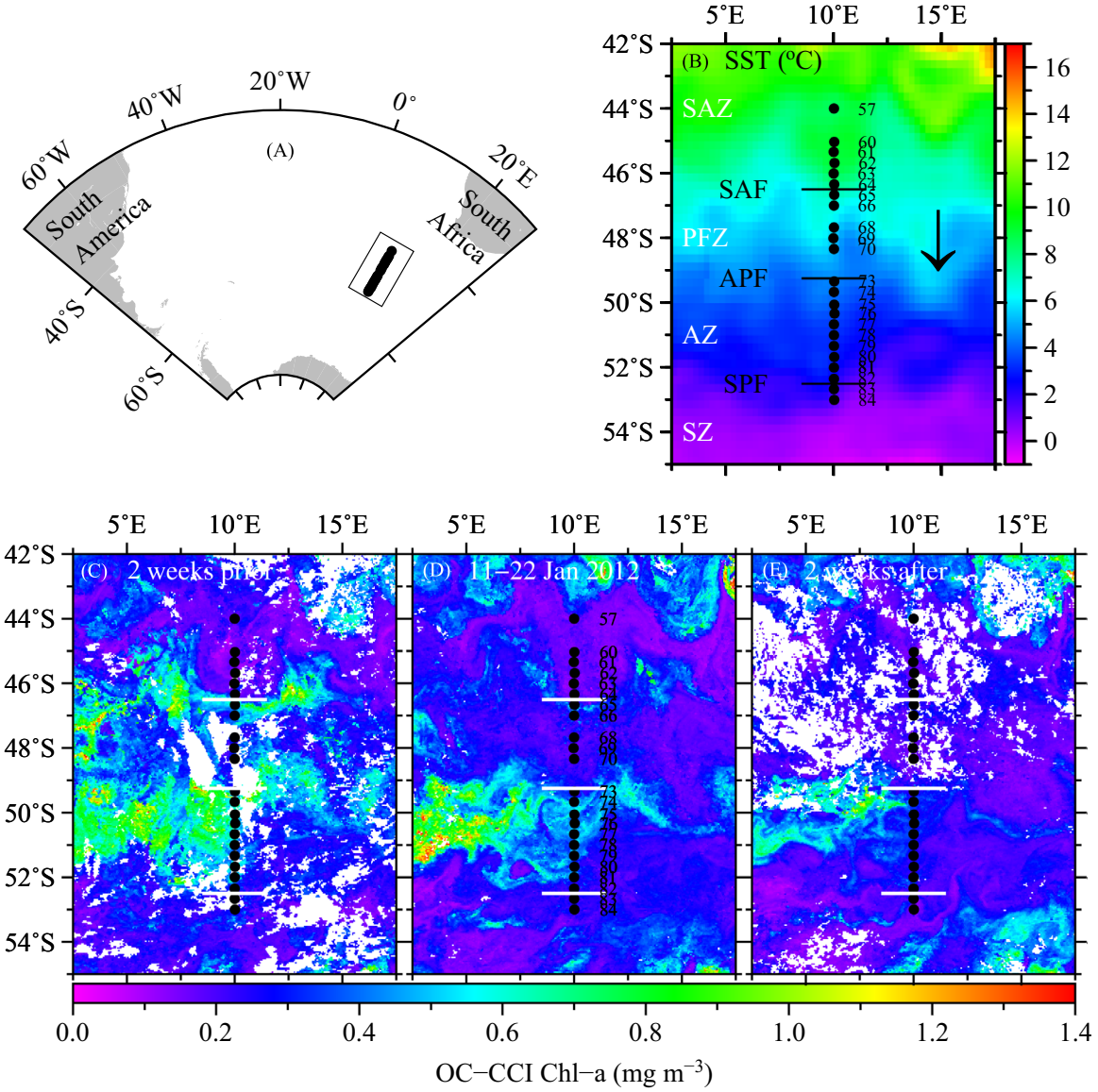

Fig. 1. (A) Map showing the location of the sampling transect southwest of South Africa (inside the rectangle symbol) in the Atlantic sector of the Southern Ocean. (B) 12-day composite images of AVHRR sea surface temperature (°C) during the sampling from 11 to 22 January 2012. Composite images of daily OC-CCI Chl-a showing the transition of the phytoplankton bloom, (C) two weeks prior to cruise, (D) during the cruise period from 11 January to 22 January 2012, and (E) two weeks after the cruise. Black arrow in (B) shows the direction of the cruise track. Black circles in (B–E) are the sampling stations. White lines in (C–E) are oceanic front positions as in (B). Sub-Antarctic Front (SAF), Antarctic Polar Front (APF), Southern Polar Front (SPF) are the major oceanic fronts observed during the cruise. SAZ, Sub-Antarctic Zone; PFZ, Polar Front Zone; AZ, Antarctic Zone; SZ, Southern Zone.

Please cite this article as: Cheah, W., et al., Importance of deep mixing and silicic acid in regulating phytoplankton biomass and community in the iron-limited.... Deep-Sea Res. II (2016), http://dx.doi.org/10.1016/j.dsr2.2016.05.019

cells (Strzepek and Harrison, 2004; van de Poll et al., 2009; Alderkamp et al., 2012). In addition, under iron-Si(OH)$_4$ co-limitation conditions, growth of non-silicious, iron-efficient phytoplankton species such as eukaryotic picoplankton and cyanobacteria often dominate over larger cells (Hutchins et al., 2001). This study aims to delineate the respective physiological responses of natural phytoplankton communities under varying nutrient and light regimes within a region subjected to CO_2 fluctuation between 45°S and 55°S along a meridional transect at 10°E in the Atlantic sector of the Southern Ocean. In particular, photophysiology of phytoplankton under iron-limitation, varying light and macronutrient concentrations conditions north and south of the APF is examined.

2. Material and methods

2.1. Study sites

Sampling was carried out as part of the "Eddy Pump - ANT-XXVIII/3" cruise along a southbound (43°S–53°S) transect centred at 10°E on board *RV Polarstern* from 11–22 January 2012 (Fig. 1). Composite images of Ocean Colour-Climate Change Initiative (OC-CCI) 4-km Chl-a (OC-CCI, 2015, http://www.oceancolour.org) show that Chl-a was in a declining stage (Fig. 1C to E). Profiles of temperature, salinity and pressure were obtained with a Seabird SBE 911plus CTD (conductivity–temperature–density) mounted on a multi-bottle water sampler. Seawater for phytoplankton pigment, absorption, nitrate+nitrite (NO_3+NO_2), PO_4, and Si(OH)$_4$ analyses was sampled from 12 L Niskin bottles (Ocean Test Equipment Inc., USA) attached to the CTD. Seawater for DFe was sampled using trace-metal clean 12 L GO-FLO bottles (General Oceanics Inc., USA), deployed independently within three hours from a CTD cast. Hydrographic features from repeated CTD casts showed that DFe sampling was carried out within the same water mass as other hydrographic sampling. Full hydrography data are available at http://doi.pangaea.de/10.1594/PANGAEA.840334.

2.2. Mixed layer depth, euphotic depth, and irradiance in the mixed layer

The mixed layer depth (z_{ML}) was defined as the first depth at which the density was 0.02 kg m^{-3} higher than the surface value (Strass et al., this issue). The euphotic depth (z_{eu}) was defined as the depth where downwelling photosynthetically active radiation (PAR) was reduced to 1% of its surface value. z_{eu} was calculated based on the PAR profiles obtained during the optical cast (Section 2.5). Prior to the calculation of z_{eu}, in situ PAR profiles were corrected for variations in solar input based on simultaneously obtained above-surface downwelling irradiance at 490 nm (E_d490) (Smith et al., 1984). E_d490 was measured at 1-min interval with a RAMSES ACC-VIS hyperspectral radiometer (TriOS GmbH, Germany) located on the uppermost deck of the ship. As surface waves can strongly affect surface PAR measurements, surface PAR at 0 m was extrapolated based on vertical light attenuation coefficient (k_d) between 5 and 21 m following the method of Stramski et al. (2008).

For stations without in situ PAR profiles, z_{eu} was calculated from vertical chlorophyll profiles measured with a fluorometer attached the CTD rosette according to the method of Morel and Maritorena (2001). Prior to the calculation of z_{eu}, chlorophyll profiles were smoothed by applying a moving median filter (Strass, 1990). Chlorophyll profiles were linearly regressed with collocated high performance liquid chromatography (HPLC)-derived total Chl-a (TChl-a). HPLC-derived TChl-a was calculated based on the sum of monovinyl Chl-a and chlorophyllide a. Divinyl Chl-a was not detected in our samples. Total daily irradiance in the mixed layer ($\overline{E}_{ML}$) was calculated as: $\overline{E}_{ML}=\overline{E}_o[1-e^{(-k_d\cdot z_{ML})}]/k_d\cdot z_{ML}$ (Boyd et al., 2007; Cheah et al., 2013). $\overline{E}_o$ is the 4-km daily surface PAR obtained from MODIS-Aqua sensor.

2.3. Nutrients

NO_3+NO_2, PO_4 and Si(OH)$_4$ were measured colorimetrically using a Technicon TRAACS 800 auto-analyzer (SEAL Analytical Limited, UK) on board the ship (Hoppe et al., this issue). DFe concentrations were determined onboard in a trace-metal clean condition according to the voltammetric method based on the electroactivity of iron complexed to dihydroxynaphthalene (Laglera et al., 2013; Puigcorbé et al., this issue).

2.4. Pigment, community structure, and absorption

Water samples (1–2 L) were collected from one to seven depths within the upper 100 m and filtered under low pressure (< 20 kPa) onto 25-mm Whatman GF/F filters. Filtered samples were then immediately shock-frozen in liquid nitrogen and stored at −80 °C until analysis. Extraction and analysis of pigments were carried out based on the method of Barlow et al. (1997) with modification customised to our instruments. In brief, pigments were extracted in 1.5 mL 100% acetone plus 50 µL of canthaxanthin as internal standard solution by homogenisation and centrifugation. Samples were analysed using a combination of a Waters 717plus autosampler, a Waters 600 controller, a LC Microsorb C8 column (100 × 4.6 mm, 3 µm), and a Waters 2998 photodiode array detector. Identification and quantification of pigments were carried out by comparing their retention times and absorption spectra using the EMPOWER software provided by Waters. Part of the pigment data were reported in Soppa et al. (2014) and are publicly available at http://doi.pangaea.de/10.1594/PANGAEA.848591.

Phytoplankton community structure was calculated using the CHEMTAX program (Mackey et al., 1996). The initial pigment ratios matrix as in Higgins et al. (2011) was applied to estimate ten taxa that generally occur in the SAZ and PFZ. The taxa were cyanobacteria, chlorophytes, prasinophytes, cyrptophytes, diatoms-1 (contain Chl-c_1, -c_2, and fucoxanthin), diatoms-2 (Chl-c_1 was replaced by Chl-c_3, typified by *Pseudonitzschia* sp.), dinoflagellates-1 (contain unambigous marker pigment peridinin), dinoflagellates-2 (containing fucoxanthin derivatives), haptophytes-6 (typified by *Emiliana* sp.), and haptophytes-8 (typified by *Phaeocystis* sp.). Data were split into three bins according to sample depth to allow for variation of pigment ratios according to irradiance. The depth bins were 0–21 m (n=41), 22–61 m (n=32), and 61–100 m (n=36), which represent 100–25%, 25–5%, and 5–0.01% of PAR, respectively. Each bin was processed separately by the CHEMTAX program using the same initial ratios matrix.

In addition, the contribution (%) of three pigment-based phytoplankton size classes (micro-, nano-, and picophytoplankton) to total phytoplankton biomass was estimated following the method of Uitz et al. (2009). Microphytoplankton (micro) correspond to phytoplankton with size > 20 µm, nanophytoplankton (nano) between 2 and 20 µm, and picophytoplankton (pico) between 0.2 and 2 µm. Fucoxanthin (Fuco), peridinin (Peri), 19′-hexanoyloxyfucoxanthin (Hex-fuco), 19′-butanoyloxyfucoxanthin (But-fuco), alloxanthin (Allo), zeaxanthin (Zea), and monovinyl chlorophyll-b (MVChl-b, divinyl chlorophyll-b was not detected in the samples) were the seven pigments chosen as diagnostic pigments (DP) representing specific phytoplankton taxa and grouped into one of the three size classes in the following equations (Uitz et al., 2009):
micro (%) = 100*((1.41*Fuco)+(1.41*Peri)/∑DP)
nano (%) = 100*((1.27*Hex-fuco)+(0.35*But-fuco)+(0.60*Allo)/∑DP)
pico (%) = 100*((0.86*Zea)+(1.01*MVChl-b)/∑DP)

Please cite this article as: Cheah, W., et al., Importance of deep mixing and silicic acid in regulating phytoplankton biomass and community in the iron-limited.... Deep-Sea Res. II (2016), http://dx.doi.org/10.1016/j.dsr2.2016.05.019

in which ∑DP represents the weighted sum of the concentrations of the seven diagnostic pigments as in:

∑DP = 1.41*Fuco + 1.41*Peri + 1.27*Hex-fuco + 0.35*But-fuco + 0.60*Allo + 0.86*Zea + 1.01*MVChl-b

Seawater from one to seven depths within the upper 100 m was filtered under low pressure (< 20 kPa) onto 47-mm Whatman GF/F filters. Filtered samples were then immediately shock-frozen in liquid nitrogen and stored at −80 °C until analysis. Measurements for particulate $[a_p(\lambda), m^{-1}]$ and detrital $[a_d(\lambda), m^{-1}]$ absorption were carried out using a Cary 4000 UV/VIS dual beam spectrophotometer equipped with a 150-mm integrating sphere (Varian Inc., USA) as described in Taylor et al. (2011). Phytoplankton absorption $[a_{ph}(\lambda), m^{-1}]$ was obtained as the difference between the a_p and a_d. Part of the phytoplankton absorption data were reported in Soppa et al. (2013) and are publicly available at http://doi.pangaea.de/10.1594/PANGAEA.819617.

2.5. Fast repetition rate fluorometry

Vertical profiles of chlorophyll fluorescence parameters of photosystem II (PSII) were measured using a FASTtracka fast repetition rate fluorometer (FRRf, Chelsea Technology Group, UK) attached to an optical cast. The optical cast also consisted of a 2π 400–700 nm integrated PAR sensor, and a pressure sensor (all from Chelsea Technology Group, UK), and a RAMSES ACC-VIS hyperspectral radiometer (TriOS GmbH, Germany) measuring downwelling irradiance. The FRRf was programmed to deliver flash sequences consisting of a series of 100 subsaturation flashlets at 1.1 µs duration and 2.8 µs intervals followed by a series of 20 relaxation flashlets (1.1 µs flash duration and 51.6 µs intervals). Fluorescence transients were then fitted to the biophysical model of Kolber et al. (1998) to yield values of minimum fluorescence (F_o), maximum fluorescence (F_m) and effective absorption cross section of PSII ($\sigma_{PSII,478}$). To differentiate parameters measured during the day from dark-adapted values, a prime (′) symbol was added to the parameters measured during the day (e.g. $\sigma'_{PSII,478}$ vs. $\sigma_{PSII,478}$). Minimum and maximum fluorescence at three stations, i.e. at 47°S, 49.3°S, and 52°S, were corrected for background fluorescence based on the averaged values of blank measurements obtained from filtered seawater (0.2 µm) collected at three depths (10 m, Chl-a maximum, 100 m). Blank samples were not available for other stations. The averaged values of the background fluorescence were < 12% of pre-corrected fluorescence values. Values of $\sigma'_{PSII,478}$ were adjusted to the in situ light spectrum according to the method of Suggett et al. (2006) as

$$\sigma'_{PSII} = \sigma'_{PSII,478}[\overline{a}(\text{in situ})]/[\overline{a}(FRRf)]$$

$\overline{a}$(FRRf) and $\overline{a}$(in situ) refer to the effective absorption coefficient determined from spectrally resolved a_{ph}, and excitation of FRRf LEDs and in situ downwelling irradiance, respectively (Suggett et al., 2006). For stations without a_{ph} measurements, $\sigma'_{PSII,478}$ values were converted to σ'_{PSII} based on the equation derived from the relationship between the ratio of $\overline{a}$(FRRf):$\overline{a}$(in situ) and optical depth (ζ) (Fig. 2) as in $\sigma'_{PSII}(z) = \sigma'_{PSII,478}(z)/[1.364 \exp -0.032\zeta]$. Non-photochemical quenching (NPQ), defined as the ratio of total non-photochemical dissipation to the rate constant for photochemistry in the light-adapted state was determined based on the normalised Stern–Volmer (NPQ_{NSV}) coefficient as: $NPQ_{NSV} = (F'_m/F'_v) - 1 = F'_o/F'_v$ (McKew et al., 2013). NPQ_{NSV} differs from the Stern–Volmer coefficient ($F_m - F'_m/F'_m$) that required both dark- and light-adapted F_m values (Olaizola et al., 1994), which does not resolve the important differences between downregulation of excitation energy transfer in high light- and low light-adapted cells (McKew et al., 2013). NPQ_{NSV} resolves these differences and is appropriate for our data set.

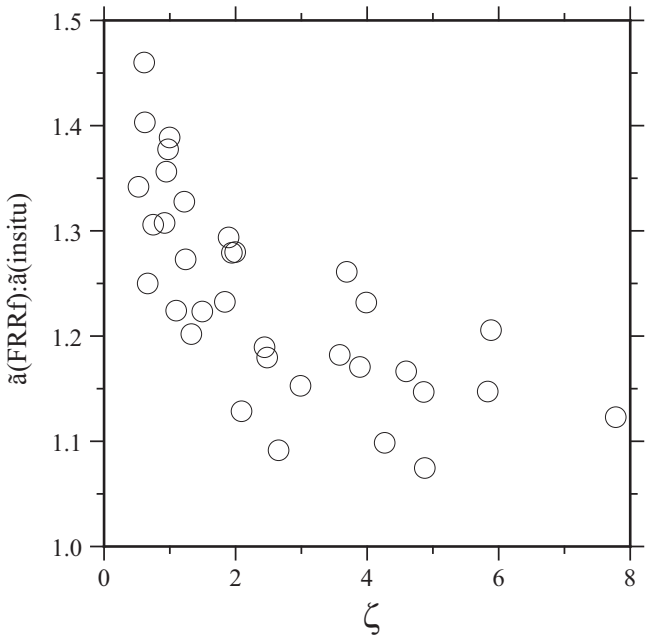

Fig. 2. The relationship between the ratio of $\overline{a}$(FRRf):$\overline{a}$(in situ) and optical depth (ζ).

2.6. Statistical analysis

Mann–Whitney *U*-test was employed to test the differences in parameters between stations north and south of the APF. Relationships between biological and environmental variables were examined using Spearman rank correlation analysis. All statistical analyses were conducted with the statistical computing software "R" (R Core Team, 2014). Principal component analysis (PCA) was applied to elucidate the influences of irradiance ($\overline{E}_{ML}$), mixing (z_{eu}/z_{ML}), nutrients ($Si(OH)_4$) on TChl-a, (DD+DT)/TChl-a and phytoplankton community structure. In order to avoid the influence of low irradiance at deeper depth only data from upper 50 m were considered in the PCA. DFe was excluded in the analysis due to low number of collocated measurements ($n = 5$). The final data matrix is composed of 26 collocated measurements and 7 variables. As the environmental and biological variables were in different units, the data were mean-centred and normalised to one standard deviation prior to the analysis.

3. Results

3.1. Hydrography

The hydrography along the 10°E transect is discussed in detail by Strass et al. (this issue). Here, we summarise some of their results that are relevant in the current context. Temperature in the upper 120 m ranged from 0.16 to 9.38 °C (Fig. 3A) with a poleward decreasing trend. Three fronts were crossed: the Sub-Antarctic Front (SAF) at 46.5°S (indicated by a sharp drop in temperature from 8 to 6 °C), the Antarctic Polar Front (APF) at 49.25°S, and the Southern Polar Front (SPF) at 52.5°S (Fig. 3). Mixed layer depths (z_{ML}) varied from 29 to 118 m with a large variation north of the APF; the shallowest and deepest z_{ML} were observed in the SAZ and PFZ, respectively (Fig. 3B). South of the APF, z_{ML} ranged from 43 to 107 m with a southward shoaling trend. z_{ML} was not significantly different between the stations north and south of the APF (Table 1).

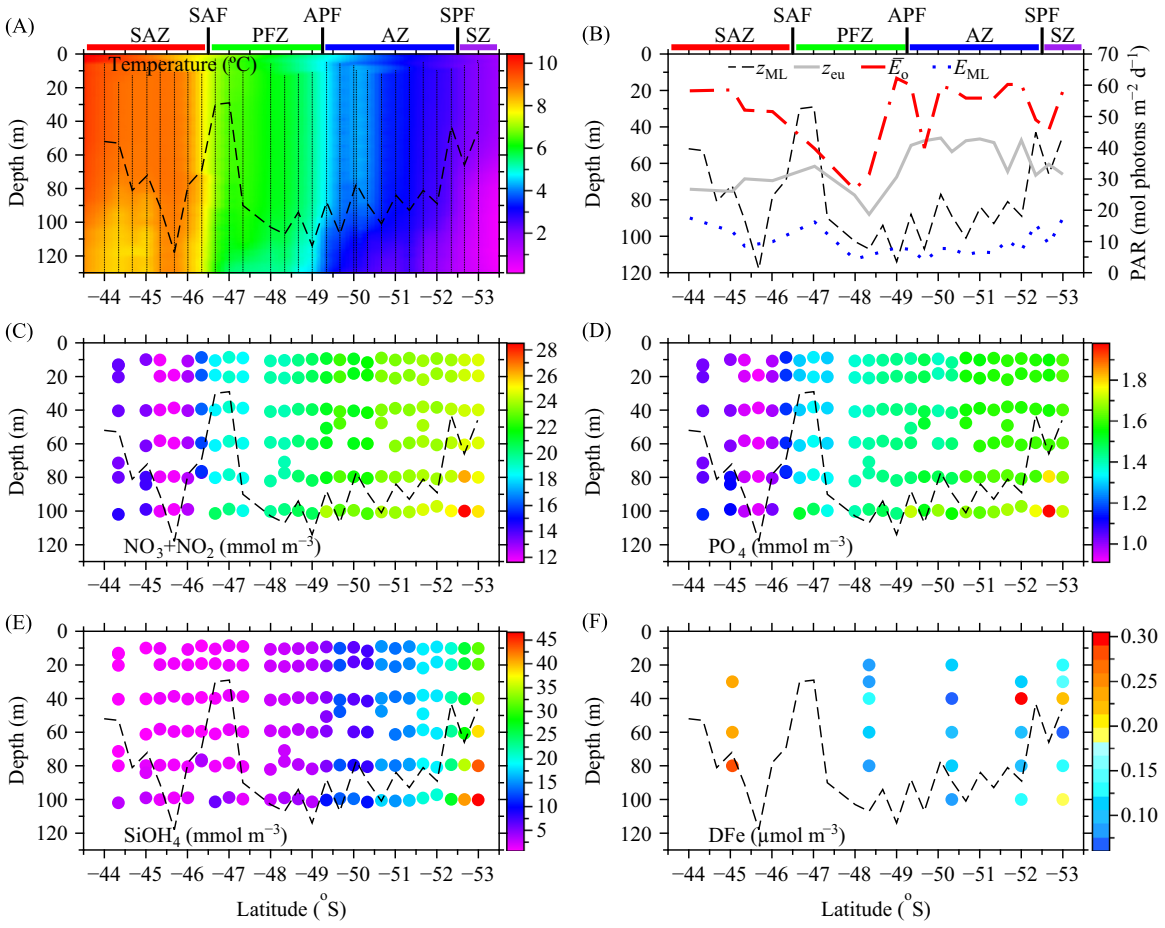

Fig. 3. Vertical structures of (A) temperature, (B) mixed layer depth (z_{ML}), euphotic depth (z_{eu}), daily surface PAR ($\overline{E}_o$), and total daily irradiance in the mixed layer ($\overline{E}_{ML}$), (C) nitrate+nitrite, (D) phosphate, (E) silicic acid, and (F) dissolved iron along the 10°E transect. Black dotted lines in panels (A) and (C–F) indicate z_{ML} as in panel (B). SAF, Sub-Antarctic Front; APF, Antarctic Polar Front; SPF, Southern Polar Front; STZ, Sub-Tropical Zone; SAZ, Sub-Antarctic Zone; PFZ, Polar Frontal Zone; AZ, Antarctic Zone.

Table 1
Mean values and Mann–Whitney *U*-test of the differences between parameters in the north and south of the APF. Significant differences are indicate in *bold*. sd, standard deviation; ns, not significant.

Parameters	North of APF		South of APF		Mann–Whitney *U*-test
	mean ± sd	*n*	mean ± sd	*n*	*p*
z_{ML}	80.7 ± 29.3	8	80.3 ± 19.8	12	0.758 (ns)
z_{eu}	72.8 ± 8.0	8	53.8 ± 8.2	12	**< 0.001**
z_{eu}/z_{ML}	1.05 ± 0.50	8	0.75 ± 0.37	12	0.070 (ns)
$\overline{E}_o$	47.5 ± 13.3	8	55.0 ± 6.6	12	0.231 (ns)
$\overline{E}_{ML}$	10.4 ± 4.8	8	8.8 ± 4.0	12	0.375 (ns)
NO_3+NO_2	16.4 ± 3.2	85	23.4 ± 1.3	75	**< 0.001**
PO_4	1.21 ± 0.19	85	1.57 ± 0.10	75	**< 0.001**
$Si(OH)_4$	1.83 ± 1.16	85	17.21 ± 9.36	75	**< 0.001**
DFe	0.15 ± 0.08	8	0.13 ± 0.06	16	0.839 (ns)
TChl-a	0.37 ± 0.12	51	0.66 ± 0.31	58	**< 0.001**
(DD+DT)/TChl-a[a]	0.20 ± 0.04	27	0.17 ± 0.04	34	**0.021**
DD+DT[a]	0.08 ± 0.03	27	0.11 ± 0.04	34	**< 0.001**
Incident PAR[a]	36.6 ± 52.6	590	181.9 ± 212.2	547	**< 0.001**
F_v/F_m	0.33 ± 0.03	68	0.36 ± 0.04	188	**< 0.001**
F_v/F_o	0.49 ± 0.07	68	0.57 ± 0.10	188	**< 0.001**
σ_{PSII}	6.59 ± 0.68	68	5.93 ± 0.70	188	**< 0.001**
$1/\tau_{Qa}$	0.17 ± 0.19	68	0.24 ± 0.08	188	**< 0.001**

[a] Only data from upper 50 m were included to avoid the influence of low irradiance at deeper depth.

3.2. Radiation

The depth of the euphotic zone (z_{eu}) ranged from 46 to 88 m along the transect and was significantly larger in waters north than south of the APF (Fig. 3B, Table 1). Along the transect, z_{ML} was mostly larger than z_{eu} in the AZ south of the APF and at stations with large z_{ML}. The ratios of z_{eu}/z_{ML}, where values below 1 indicate mixed waters and values above 1 indicating stratified waters (Uitz et al., 2008), were higher in the north (1.05 ± 0.50) than south (0.75 ± 0.37) of the APF, although the differences were not significant (Table 1).

Daily surface PAR ($\overline{E}_o$) was ~50 mol photons m^{-2} d^{-1} in the SAZ and dropped to ~30 mol photons m^{-2} d^{-1} in the PFZ. In the AZ, $\overline{E}_o$ increased to ~55 mol photons m^{-2} d^{-1} (Fig. 3B). On average, $\overline{E}_o$ was not significantly different north and south of the APF (Table 1). Total daily irradiance in the mixed layer ($\overline{E}_{ML}$) ranged between 3.9 and 17.5 mol photons m^{-2} d^{-1} along the transect whereby $\overline{E}_{ML}$ > 10 mol photons m^{-2} d^{-1} have been observed at stations both north and south of the APF (Fig. 3B). Mean $\overline{E}_{ML}$ values were 10.4 ± 4.8 in waters north of the APF and 8.8 ± 4.0 in the south of the APF. High $\overline{E}_{ML}$ were generally recorded at stations with shallower z_{ML}. No significant differences were observed between $\overline{E}_o$ values recorded north and south of the APF (Table 1).

Concentrations of NO_3+NO_2 within the upper 100 m were always > 11.5 mmol m^{-3} along the transect (Fig. 3C). Although concentrations of NO_3+NO_2 were replete across the whole

transect, a sharp increase from north to south in NO_3+NO_2 can clearly be observed across all three fronts i.e. SAF, APF, and SPF. NO_3+NO_2 concentrations in waters south of the APF were significantly higher than those in waters north of the APF with mean values of 23.4 ± 1.3 mmol m^{-3} and 16.4 ± 3.2 mmol m^{-3}, respectively (Table 1). The vertical structure of NO_3+NO_2 within the upper 100 m was very uniform except in the Southern Zone (SZ) in which NO_3+NO_2 concentrations were higher below the mixed layer. PO_4 concentrations ranged from 0.92 to 1.98 mmol m^{-3} with similar spatial and vertical distributions as NO_3+NO_2 and higher concentrations observed further south (Fig. 3D). The region with slightly lower concentrations in PO_4 ($\sim$0.9 mmol m^{-3}) coincides with lower NO_3+NO_2 concentrations ($\sim$11.8 mmol m^{-3}) at 45.3°S −46°S in the SAZ. Concentrations of $Si(OH)_4$ exhibit a distinctive pattern across the APF. In waters north of the APF, $Si(OH)_4$ concentrations were depleted with a mean concentration of only 1.83 ± 1.16 mmol m^{-3} (Table 1). At the APF, concentrations of $Si(OH)_4$ increased to $\sim$5 mmol m^{-3} (Fig. 3E). South of the APF, $Si(OH)_4$ concentrations were much higher with a mean concentration of 17.21 ± 9.36 mmol m^{-3}. $Si(OH)_4$ concentrations were generally uniform within the mixed layer. Concentrations of dissolved iron (DFe) within the upper 100 m were typically low across the whole transect varying between 0.060 and 0.305 μmol m^{-3} (Fig. 3F). Strong depletion in DFe concentrations (<0.12 μmol m^{-3}) was observed in waters close to the APF, between south of the PFZ and north of the AZ (48°S −51°S). DFe concentrations $>$ 0.2 μmol m^{-3} were recorded in the SAZ, south of the AZ, and in the SZ. As with NO_3, concentrations of PO_4 and $Si(OH)_4$ were significantly higher at stations south of the APF than north of the APF,

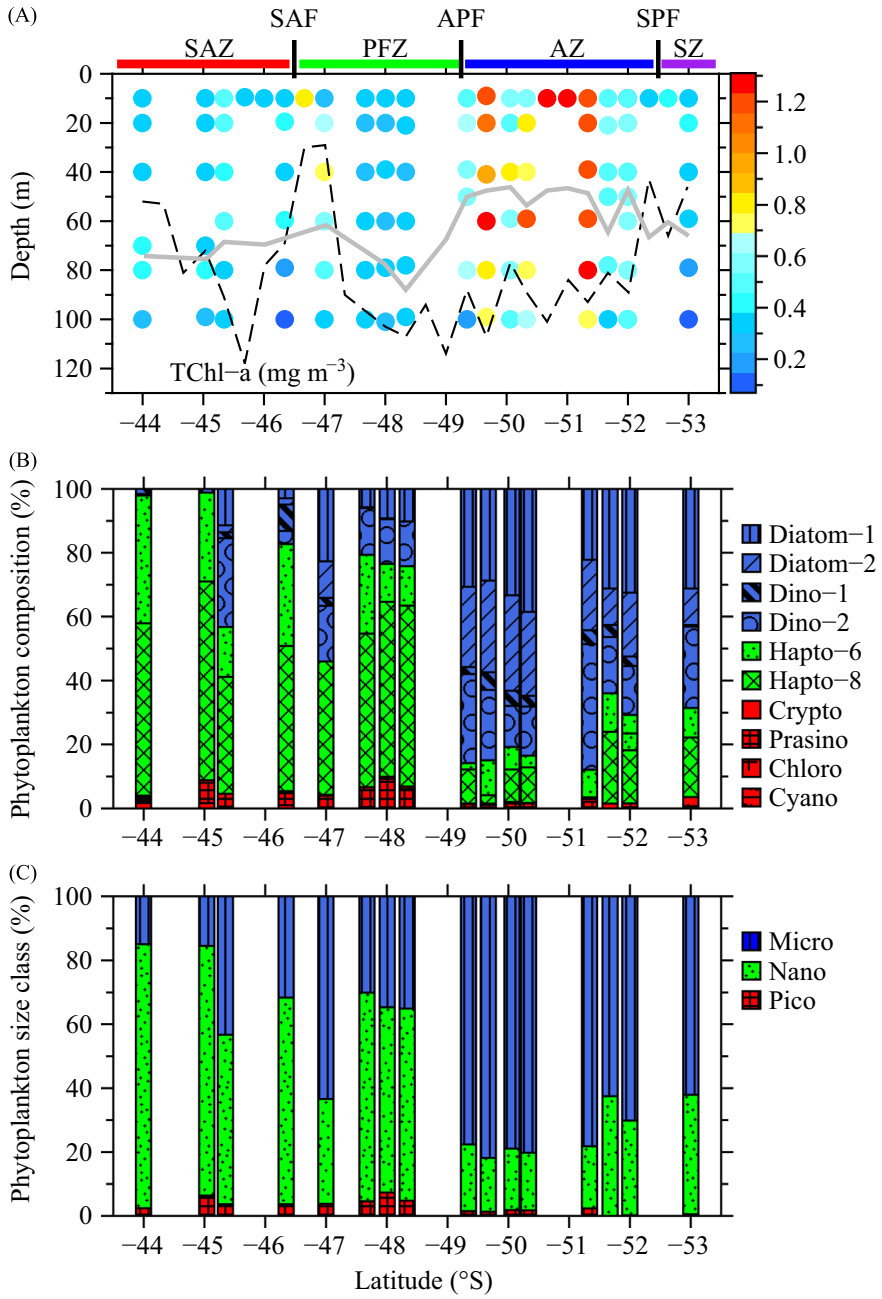

Fig. 4. (A) TChl-a concentrations, relative contribution (%) of 100-m integrated (B) phytoplankton taxa, and (C) size classes along the transect. Black dotted line and grey solid line in panel (A) indicate z_{ML} and z_{eu}, respectively. SAF, Sub-Antarctic Front; APF, Antarctic Polar Front; SPF, Southern Polar Front; STZ, Sub-Tropical Zone; SAZ, Sub-Antarctic Zone; PFZ, Polar Frontal Zone; AZ, Antarctic Zone; SZ, Southern Zone.

Please cite this article as: Cheah, W., et al., Importance of deep mixing and silicic acid in regulating phytoplankton biomass and community in the iron-limited.... Deep-Sea Res. II (2016), http://dx.doi.org/10.1016/j.dsr2.2016.05.019

Table 2
Relationships between biological parameters and environmental properties for all stations. Significant correlations at 95% significance level are indicated in **bold**.

Parameters	All stations		
	r	*p*	*n*
TChl-a vs. z_{eu}/z_{ML}[a]	**−0.65**	0.014	14
TChl-a vs. $Si(OH)_4$[a]	0.275	0.341	14
TChl-a vs. $Si(OH)_4$[b]	**0.59**	0.036	13
Microphytoplankton vs. NO_3+NO_2	**0.55**	< 0.001	83
Microphytoplankton vs. PO_4	**0.57**	0.000	83
Microphytoplankton vs. $Si(OH)_4$	**0.52**	< 0.001	83
Nanophytoplankton vs. NO_3+NO_2	**−0.54**	< 0.001	83
Nanophytoplankton vs. PO_4	**−0.56**	< 0.001	83
Nanophytoplankton vs. $Si(OH)_4$	**−0.51**	< 0.001	83
(DD+DT)/TChl-a vs. Microphytoplankton[c]	**−0.40**	0.002	58
(DD+DT)/TChl-a vs. Nanophytoplankton[c]	**0.41**	0.002	58
F_v/F_m vs. Microphytoplankton	**0.31**	0.003	25
F_v/F_m vs. Nanophytoplankton	**−0.35**	0.002	25
Dinoflagellates-2 vs. chlorophyllide-a	**0.73**	< 0.001	104
Haptophytes-8 vs. chlorophyllide-a	**−0.40**	< 0.001	104

[a] 100 m-integrated data.
[b] 100 m-integrated data from all stations except data from 53° in the SZ.
[c] Only data from upper 50 m were included to avoid the influence of low irradiance at deeper depth.

whereas DFe concentrations were not significantly different between the stations (Table 1).

3.3. Phytoplankton pigment and community composition

Along the 10°E transect, TChl-a concentrations within the upper 100 m ranged from 0.07 to 1.31 mg m^{-3} (Fig. 4A) with mean TChl-a concentration in waters north of the APF (0.37 ± 0.12 mg m^{-3}) only half and significantly lower than the mean TChl-a concentration in waters south of the APF (0.66 ± 0.31 mg m^{-3}, Table 1). In the SAZ and PFZ north of the APF, concentrations of TChl-a were typically between 0.2 and 0.4 mg m^{-3} except at 45.3°S and 47°S, where the TChl-a concentrations were higher with 0.5 mg m^{-3} and 0.8 mg m^{-3}, respectively. South of the APF, TChl-a concentrations were mostly higher than 0.5 mg m^{-3} except in the SZ (Fig. 4A). TChl-a concentrations > 1 mg m^{-3} were confined to the AZ south of the APF at around 49.7°S, and between 50.3°S and 51.3°S, where z_{ML} was larger than z_{eu}. Significant negative correlation was observed between TChl-a and z_{eu}/z_{ML} ratio (Table 2), indicating that phytoplankton blooms were confined to well-mixed waters. The correlation between 100 m-integrated TChl-a and $Si(OH)_4$ was not significant, due mainly to low TChl-a concentrations in the SZ (Fig. 4A). However, when data from the SZ was excluded, a significant positive correlation between TChl-a and $Si(OH)_4$ was obtained (Table 2).

A distinctive phytoplankton community structure was observed north and south of the APF (Fig. 4B). North of the APF, dominance of haptophytes up to 90% was recorded in the north of the SAZ. Contribution of haptophytes gradually reduced southward but it maintained a strong dominance of ~70–80% in the PFZ except at 45.3°S and 47°S, where the contribution of haptophytes dropped to about 40–50%. Coincidentally, these two stations also reported an increase in TChl-a concentration (Fig. 4A) and the highest contribution of diatoms (13–24%) and dinoflagellates-2 (20–29%, heterotrophic) in waters north of the APF (Fig. 4B). At taxa level, waters north of the APF were dominated by *Phaeocystis* sp. as indicate by a high contribution of haptophytes-8. South of the APF, diatoms-1 was the dominant group contributing about 22–39% of total biomass, followed by diatoms-2 (~11–30%, typified by *Pseudonitzschia* sp.) and heterotrophic dinoflagellates-2 (~6–40%). Vertical profiles of phytoplankton community structure show at stations south of the APF, dominance of diatoms-2 (*Pseudonitzschia* sp.) widespread within the 100 m water column (Fig. 5B). A similar distribution was observed for dinoflagellates-1 (Fig. 5C). In contrast, the vertical distribution of haptophytes-8 shows higher contribution at the surface than at depth in the north of the APF (Fig. 5F). Contribution of prasinophytes were higher in the PFZ than in other zones (Fig. 5G).

Distribution of pigment-based phytoplankton size classes exhibits similar trends as in phytoplankton groups with nanophytoplankton dominating north of the APF and waters south of the APF were dominated by macrophytoplankton (Fig. 4C). Overall, cyanobacteria and picophytoplankton contribute less than 10% of total biomass along the transect. Contrasting relationships were obtained between different phytoplankton size classes and macronutrients (Table 2). As expected, positive correlations were obtained between macronutrients and microphytoplankton and negative with nano- and picophytoplankton, suggesting that macronutrients were driving the succession of bigger cells along the transect. Two types of Chl-a degraded products, chlorophyllide-a and pheophorbide-a, were observed in this study. High ratios of chlorophyllide-a/TChl-a were observed at all high TChl-a stations along the transect (Fig. 6A), whereas ratios of pheophorbide-a/TChl-a were only recorded at high TChl-a stations south of the APF (Fig. 6B).

3.4. Photoprotective pigments

Ratios of the photoprotective xanthophyll cycle pigments, diadinoxanthin (DD)+diatoxanthin (DT)/TChl-a ((DD+DT)/TChl-a) were generally higher at the surface and ranged from 0.12 to 0.28 within the upper 20 m (Fig. 6C). A more profound decrease in (DD+DT)/TChl-a ratios below the mixed layer was observed at stations with shallower mixed layer than at those with deep mixed layer. At the deep mixed layer stations, (DD+DT)/TChl-a ratios higher than 0.10 can be observed down to 80–100 m along the transect. The different vertical patterns in (DD+DT)/TChl-a ratios reflect the influence of water stratification on photoacclimation strategy of phytoplankton. (DD+DT)/TChl-a ratios in waters north of the APF were significantly higher than those in the south (Table 1). High ratios of (DD+DT)/TChl-a in waters north of the APF were due to low TChl-a as DD+DT concentrations were significantly higher in waters south of the APF (Table 1). There was a significant negative correlation between (DD+DT)/TChl-a and microphytoplankton, and a significant positive correlation with nanophytoplankton along the transect indicating that nanophytoplankton, in particular haptophytes, were producing more photoprotective pigments and less TChl-a than macrophytoplankton.

3.5. Biophysical PSII parameters

The values of overall actual operating efficiency of PSII under ambient light (F'_q/F'_m) varied from 0.01 to 0.44 in the upper 100 m, and were low (0.01–0.15) from the surface down to around 30 m at most of the stations, reflecting the influence of high light at the surface. At 48.3°S, due to low surface incident PAR (Fig. 6D), surface F'_q/F'_m values were around 0.20 (Fig. 6E). Below 30 m, F'_q/F'_m gradually increased with values ranging from 0.15 to 0.30 within the mixed layer. F'_q/F'_m higher than 0.35 were only observed either near the z_{ML} or below the z_{ML} in which maximum F'_q/F'_m of 0.44 was observed below the z_{ML} at 95 m at Station 84 (53°S) south of the APF (Fig. 6E). Maximum efficiency of PSII in the dark (F_v/F_m) ranged from 0.23 to 0.49 with lower values at the surface (0.26–0.38) and increased with depth reaching the maximum value of 0.49 at around 98 m at Station 81 (52°S, data not shown). The mean F_v/F_m in waters north of the APF was 0.33 ± 0.03 which was significantly lower than mean F_v/F_m value (0.36 ± 0.04) in waters south of the APF (Table 1). Mean F_v/F_o, which represents the

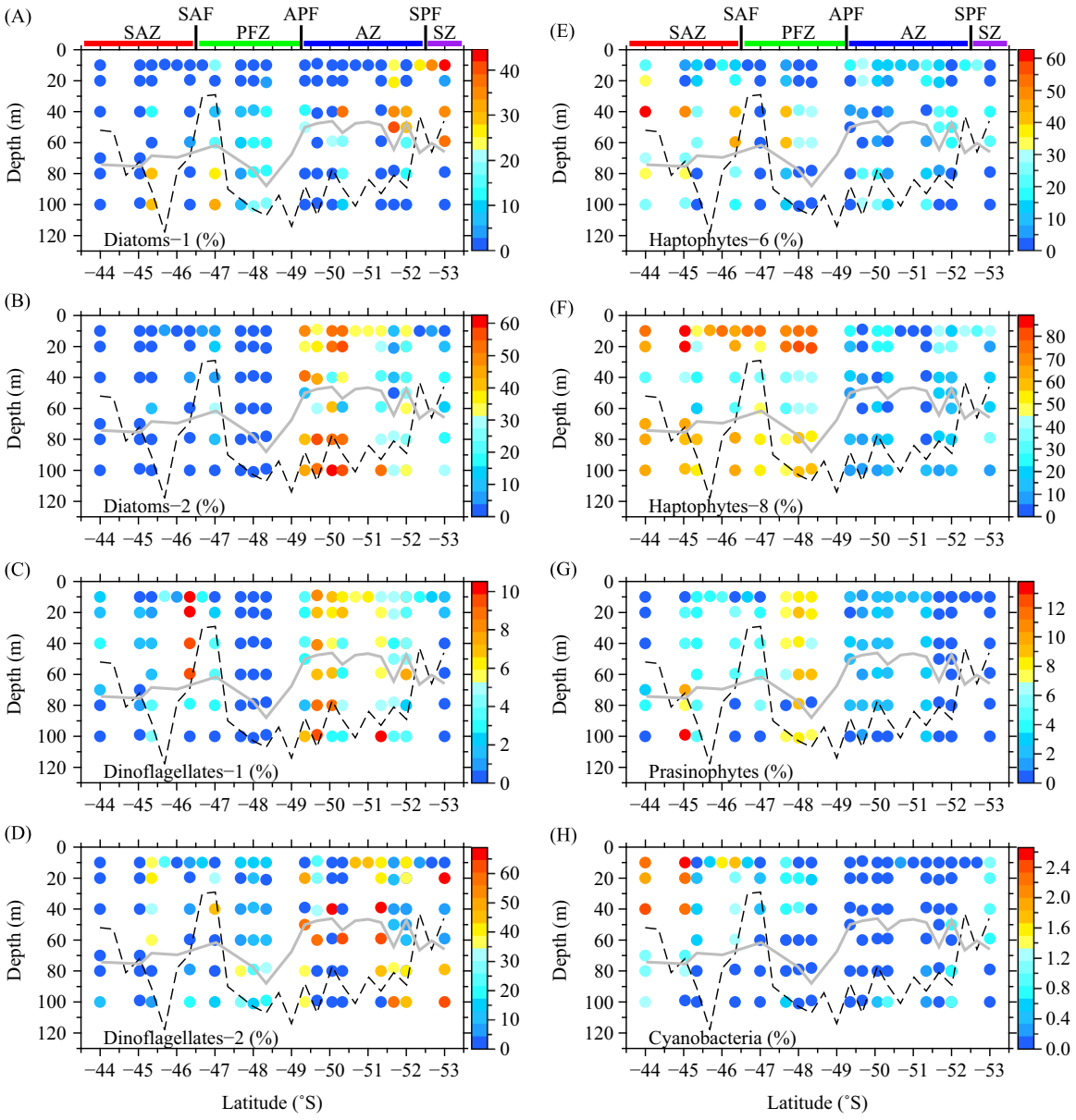

Fig. 5. (A) Vertical structures of relative contribution (%) of major phytoplankton taxa along the transect. Black dotted lines and grey solid lines in all panels indicate z_{ML} and z_{eu}, respectively. SAF, Sub-Antarctic Front; APF, Antarctic Polar Front; SPF, Southern Polar Front; STZ, Sub-Tropical Zone; SAZ, Sub-Antarctic Zone; PFZ, Polar Frontal Zone; AZ, Antarctic Zone; SZ, Southern Zone.

proportion of functional PSII reaction centres (RCII), was significantly higher in waters south of the APF (0.49 ± 0.07) than those in the north of the APF (0.57 ± 0.10; Table 1).

The values of effective absorption cross section of PSII under ambient light (σ'_{PSII}) varied from 1.17 to 8.89 nm^2 and showed similar vertical distribution as in F'_q/F'_m with low values at the surface extending to 50 m within the mixed layer and increased below the mixed layer (Fig. 6F). Effective absorption cross section of PSII in the dark (σ_{PSII}) ranged between 4.20 and 8.83 nm^2 with a significantly higher mean value in waters north of the APF than south of the APF (Table 1). No significant correlations were observed between DFe, F_v/F_m and σ_{PSII} along the transect. Incindentally, F_v/F_m were observed to correlate positively with microphytoplankton and negatively with nanophytoplankton (Table 2). The rate constant for reopening of closed RCII ($1/\tau_{Qa}$), determined from the inverse of the turnover time for PSII, were significantly lower in waters north of the of APF (0.17 ± 0.19 ms^{-1}) than in the south (0.23 ± 0.08 ms^{-1}, Table 1).

High values of NPQ_{NSV} were observed at stations under the influence of high incident PAR within the upper 50 m (Fig. 6D & G) in both north and south regions of the APF (Table 3). Correspondingly, significant positive correlations were also obtained between (DD+DT)/TChl-a and incident PAR in both regions across the APF. This is expected given the photoprotective role of the xanthophyll cycle pigments in dissipating excessive energy under high irradiance condition via non-photochemical quenching. Interestingly, only the region north of the APF shows significant positive correlation between NPQ_{NSV} and (DD+DT)/TChl-a (Table 3), although high NPQ_{NSV} values were recorded across the whole transect. In contrast to NPQ_{NSV}, values of F'_q/F'_v, which accounts for the proportion of RCII in the "open" state, were low at the surface and increased at further depth when the influence of PAR is negligible (Fig. 6H).

Please cite this article as: Cheah, W., et al., Importance of deep mixing and silicic acid in regulating phytoplankton biomass and community in the iron-limited.... Deep-Sea Res. II (2016), http://dx.doi.org/10.1016/j.dsr2.2016.05.019

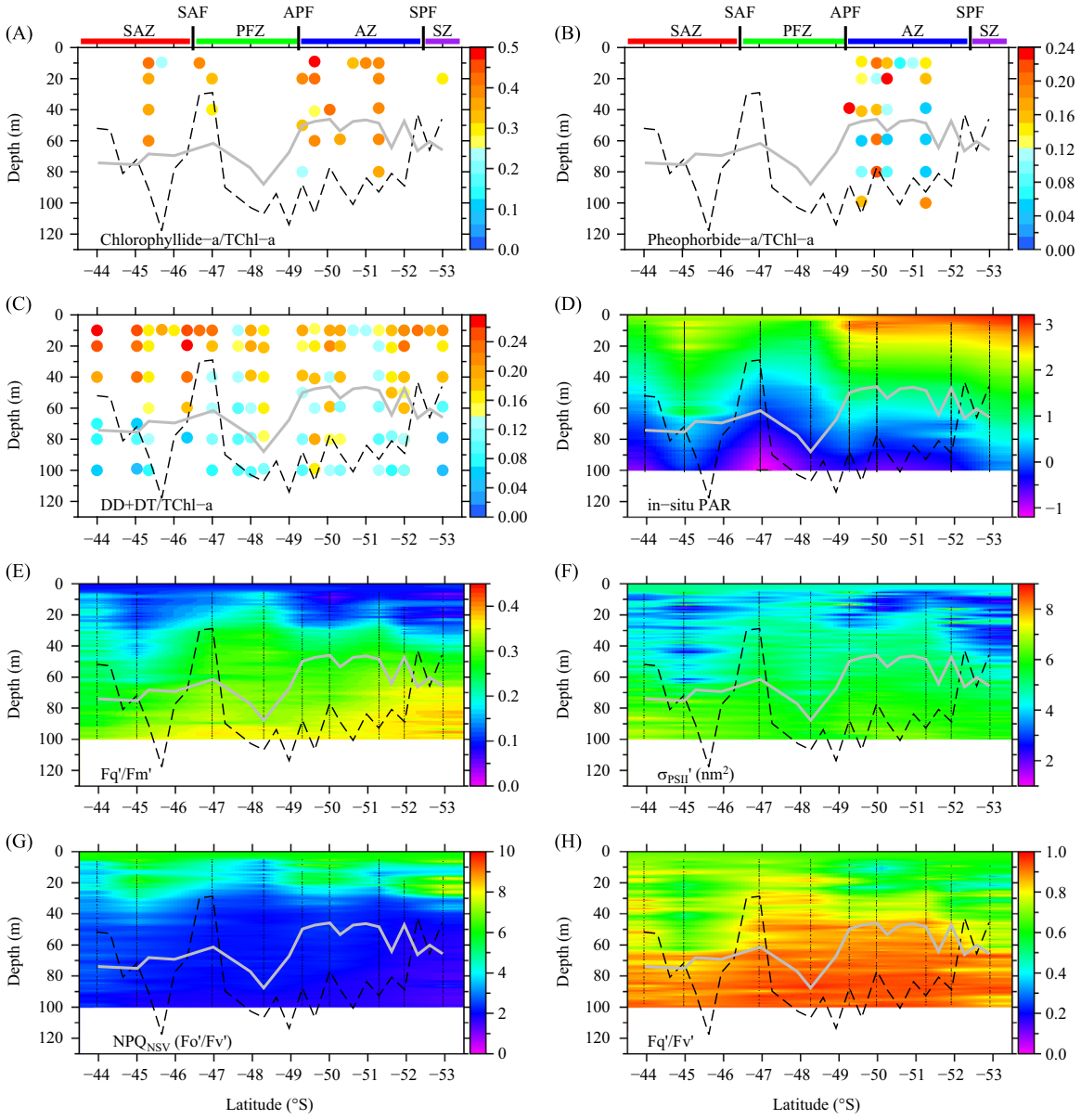

Fig. 6. Vertical structures of the concentrations of Chl-a degraded products (A) chlorophyllide-a and (B) pheophorbide-a. (C) Total photoprotective pigments in the xanthophyll cycle ((DD+DT)/TChl-a). (D) Log(base 10)-transformed incident PAR (μmol photons m^{-2} s^{-1}). (E) Overall actual operating efficiency of PSII under ambient light (F'_q/F'_m) and (F) functional absorption cross section of PSII (σ'_{PSII}) under ambient light. Black dotted lines and grey solid lines in all panels indicate z_{ML} and z_{eu}, respectively. SAF, Sub-Antarctic Front; APF, Antarctic Polar Front; SPF, Southern Polar Front; STZ, Sub-Tropical Zone; SAZ, Sub-Antarctic Zone; PFZ, Polar Frontal Zone; AZ, Antarctic Zone; SZ, Southern Zone.

Table 3
Relationships between biological and environmental parameters in regions north and south of the APF. Significant correlations at 95% significance level are indicated in *bold*.

Parameters	North of APF			South of APF		
	r	*p*	*n*	*r*	*p*	*n*
NPQ_{NSV} vs. incident PAR[a]	**0.82**	< 0.001	164	**0.91**	< 0.001	187
NPQ_{NSV} vs. (DD+DT)/TChl-a[a]	**0.76**	0.016	10	0.57	0.200	7
(DD+DT)/TChl-a vs. incident PAR[a]	**0.72**	0.011	12	**0.61**	0.024	14

[a] Only data from upper 50 m were included to avoid the influence of low irradiance at deeper depth.

Table 4
Results of principal component analysis. Significant correlations at 95% significance level ($p < 0.05$) among variables within each PC are indicated in *bold*.

Component	PC1	PC2
Variation (%)	49.1	23.9
z_{eu}/z_{ML}	**−0.87**	−0.26
$\overline{E}_{ML}$	**−0.59**	**−0.50**
SiO_4	**0.40**	**−0.66**
Microphytoplankton	**0.89**	−0.11
Nanophytoplankton	**−0.89**	0.13
TChl-a	**0.87**	−0.14
(DD+DT)/TChl-a	**−0.49**	**0.42**

3.6. *Multivariate analysis*

Relationships among phytoplankton and key environmental variables across the APF were examined using PCA. The results of the PCA show that the first two principal components account for 73.0% of the total variance of the data set, in which the first component (PC1) alone is accounting for almost half of the total variance (Table 4). Significant variable loadings for PC1 were

Please cite this article as: Cheah, W., et al., Importance of deep mixing and silicic acid in regulating phytoplankton biomass and community in the iron-limited.... Deep-Sea Res. II (2016), http://dx.doi.org/10.1016/j.dsr2.2016.05.019

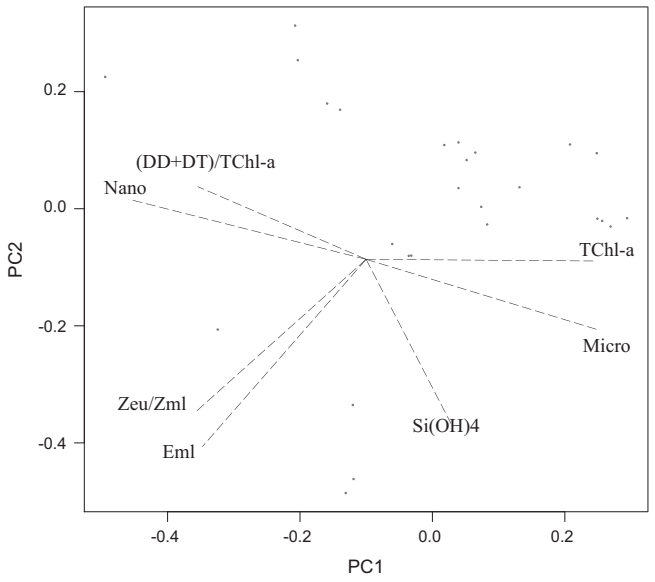

Fig. 7. Principal Component Analysis loading scores for the two principal components.

positive for microphytoplankton, TChl-a, and $Si(OH)_4$, and negative for z_{eu}/z_{ML}, $\overline{E}_{ML}$, nanophytoplankton, and (DD+DT)/TChl-a). The PC1 is thus primarily influenced by the mixing status, community composition, TChl-a, and photoacclimation response (Fig. 7). The main variables that form the second component (PC2) are $\overline{E}_{ML}$, $Si(OH)_4$, and (DD+DT)/TChl-a. This shows that PC2 mostly represents the photoacclimation processes and nutrients. The results of the PCA reinforced the view that phytoplankton biomass and community composition in the APF region were related to mixing and $Si(OH)_4$ status.

4. Discussion

4.1. State of the phytoplankton bloom

Although TChl-a concentrations >1 mg m^{-3} can be observed in waters south of the APF, satellite images before and after the cruise show that the phytoplankton bloom was at a declining stage during sampling. High concentrations of degraded Chl-a products, i.e. chlorophyllide-a and pheophorbide-a at high TChl-a stations indicate a declining bloom (Wright et al., 2010). Chlorophyllide-a and pheophorbide-a can be produced from senesced phytoplankton or by mastication during grazing (Louda et al., 1998; Wright et al., 2010). The high contribution of dinoflagellates-2 observed only at high TChl-a stations (Fig. 4A) suggests that grazing activity by heterophic dinoflagellates was taking place at these stations (Fig. 4B). It should be noted that dinoflagellates-2 lack unique diagnostic pigments and contain Fuco and Hex-fuco as their main caretenoids, which are shared by a number of taxa, notably haptophytes (Wright et al., 2010; de Salas et al., 2011). Nevertheless, a significant positive correlation was observed between chlorophyllide-a and dinoflagellates-2, and a negative correlation between chlorophyllide-a and haptophytes-8 (Table 2), indicating that chlorophyllide-a concentrations at high TChl-a stations were not contributed by haptophytes. High concentrations of heterotrophic flagellates have also been reported across the SAZ and PFZ in the Southern Pacific Ocean (de Salas et al., 2011), which are one of the major grazers in those regions (Pearce et al., 2011).

4.2. Indications of iron limitation

With a maximum achievable F_v/F_m value of ca. 0.65 under optimal nutrient replete conditions (Kolber and Falkowski, 1993), low mean F_v/F_m (<0.40) values observed across the north and south regions of the APF could be attributed to iron limitation. Low mean values of $1/\tau_{Qa}$ (<0.3 m s^{-1}) across the APF suggest that there was a large proportion of reduced plastoquinone pool (McKew et al., 2013), which could have resulted from a large proportion of reduced RCII. Laboratory and ship-board iron fertilisation experiments have reported an increase in F_v/F_m to >0.5 and $1/\tau_{Qa}>0.3$ m s^{-1} in response to iron addition (Greene et al., 1992; Kolber et al., 1994; Moore et al., 2007). Studies have shown that diatoms are capable of coping with low iron conditions by reducing the concentrations of iron-demanding cellular components such as cytochrome b_6f (cyt b_6f) and photosystem I (PSI) protein complexes, which are electron acceptors downstream of PSII (Greene et al., 1992; Strzepek and Harrison, 2004). As a result, low concentrations of these electron acceptors will result in a large proportion of RCII remaining in a reduced state, lowering F_v/F_m and $1/\tau_{Qa}$ (Greene et al., 1992).

4.3. Phytoplankton assemblages under low and modest silicic acid concentrations

Under NO_3+NO_2-, PO_4-replete, and DFe-limited conditions, $Si(OH)_4$ plays a significant role in controlling phytoplankton biomass and community structure across the APF regions as indicated in the significant positive correlations between $Si(OH)_4$, TChl-a, and microphytoplankton. In waters north of the APF, low mean $Si(OH)_4$ concentration (<2 mmol m^{-3}) suggests that cells were probably suffering from $Si(OH)_4$ deficiency (Franck et al., 2000). As a consequence, $Si(OH)_4$ limitation leads to the dominance of smaller nanophytoplankton mainly haptophytes, which usually prevail over larger cells under $Si(OH)_4$ limitation condition (Hutchins et al., 2001). In contrast, sufficient supply of $Si(OH)_4$ (>5 mmol m^{-3}) in waters south of the APF lead to high TChl-a concentrations and diatom-dominated phytoplankton community structure.

4.4. Influence of light in the shallow and deep mixed layer

The relatively weaker contrast in vertical distribution of (DD+DT)/TChl-a ratios within the mixed layer at stations with deeper mixed layer, i.e. $z_{ML}>z_{eu}$ shows that phytoplankton in well-mixed waters spent more time in the deeper parts of the mixed layer receiving less light. The corresponding higher values of σ'_{PSII} within the mixed layer and low $\overline{E}_{ML}$ concentrations indicate that phytoplankton at these stations on average spent more time in a relatively low irradiance environment. This suggests that during the mixing process, phytoplankton at deep mixed layer stations were exposed to a range of irradiance intensities and acclimating to lower levels of irradiance. Laboratory experiments have shown that diatoms and haptophytes exposed to fluctuation in irradiance are acclimating to lower irradiances than cells grown under constant irradiance (van de Poll et al., 2007, 2009). This could explain the lower ratios of DD+DT to TChl-a at these stations. In contrast, phytoplankton at shallower mixed layer stations were trapped within a shallower and more stratified water column, and therefore were exposed to higher light intensity. Consequently, phytoplankton at these stations were producing more photoprotective pigments at the expense of Chl-a. The findings of PCA and the significant negative correlations between 100-m integrated TChl-a and z_{eu}/z_{ML} at all stations (Table 2), which shows that TChl-a concentrations were lower at shallower and more stratified stations, confirm that this is the case.

Please cite this article as: Cheah, W., et al., Importance of deep mixing and silicic acid in regulating phytoplankton biomass and community in the iron-limited.... Deep-Sea Res. II (2016), http://dx.doi.org/10.1016/j.dsr2.2016.05.019

DD and DT are the main photoprotective xantophyll cycle pigments widespread in diatoms, haptophytes and dinoflagellates. DD pigment will assist in light harvesting by transferring energy to chlorophylls under lower light condition, whereas under intense light, DD will be converted to DT to shield off excessive light energy via NPQ. The DD+DT xanthophyll cycle and NPQ operate as a rapid photoacclimation mechanism regulating between light harvesting and thermal dissipation of excess light energy under rapid light fluctuation conditions (Brunet and Lavaud, 2010; Goss and Jakob, 2010). Low values of F'_q/F'_m, F'_q/F'_v, and σ'_{PSII} in response to high incident PAR at the surface indicate that a large proportion of RCII were reduced. Large fraction of reduced RCII under high irradiance conditions have shown to increase the capacity of NPQ and reduce the risk of photodamage (Moore et al., 2006). Our results indicate that xanthophyll cycling and NPQ provide a cost-effective short-term photoprotection mechanisms that are vital to phytoplankton living in the iron-limited and rapid light fluctuation environment in the APF.

4.5. Contrasting photoacclimation response in haptophytes- and diatoms-dominated community

In the haptophyte-dominated region north of the APF, the ratios of (DD+DT)/TChl-a were significantly higher than in the south despite being exposed to lower incident PAR and similar $\overline{E}_{ML}$ levels (Table 1, Fig. 7). As DFe concentrations were not significantly different between the regions in the north and south of the APF, differences in the ratios of (DD+DT)/TChl-a may originate from taxon-specific response to light. Studies have shown that haptophytes are better adapted to low light and are more prone to photoinhibition compared to diatoms that are better acclimated to high light (Arrigo et al., 2000; Kropuenske et al., 2010). The study by Alderkamp et al. (2012) has also shown that haptophytes produced higher ratios of (DD+DT)/TChl-a than diatoms under iron-limited conditions. Similarly, significantly lower F_v/F_m, F_v/F_o, $1/\tau_{Qa}$, and higher σ_{PSII} observed in the region north of the APF could have been due to the high abundance of nanophytoplankton in this region. Phytoplankton with smaller cell size have shown to exhibit lower F_v/F_m and higher σ_{PSII} than larger phytoplankton such as diatoms (Suggett et al., 2009). In this study, nanophytoplankton correlate positively with (DD+DT)/TChl-a and negatively with F_v/F_m (Table 2), suggesting that higher (DD+DT)/TChl-a ratios and lower F_v/F_m observed in the region north of the APF may be due to the dominance of smaller size phytoplankton in this region.

5. Conclusion

Our findings show that in addition to iron, other factors such as light, mixed layer depth, $Si(OH)_4$, and photoacclimation response of phytoplankton also play important roles in regulating TChl-a concentrations in the APF. Overall, under iron-limited conditions, phytoplankton across the APF were more prone to high light, especially for cells living in a shallow mixed layer (<60 m) environment and were producing more photoprotective pigments at the expense of Chl-a. Across the APF, even though the influence of $Si(OH)_4$ was confined to taxonomic level, the subsequent photoacclimation response of different phytoplankton groups driven by $Si(OH)_4$, in turn, was influencing the concentrations of TChl-a in the regions north and south of the APF. Based on our findings, we propose that high TChl-a concentrations (>0.6 mg m^{-3}) are achievable even for iron-limited phytoplankton living in the vicinity of the APF during late summer, if $z_{ML}>60$ m, $z_{eu}/z_{ML}<1$, and $Si(OH)_4$ is not in limiting conditions, i.e. >5 mmol m^{-3}.

Acknowledgement

We would like to thank the captain and crew of RV Polarstern and fellow expeditioners for their assistance during the ANT-XVIII/III "Eddy-Pump" cruise. We thank NASA for providing MODIS Chl-a and PAR data, and SeaWiFS Chl-a data, and NOAA for the AVHRR data. We also thank ESA for the MERIS Chl-a data and the OC-CCI merged Chl-a data. We are indebted to Dr. Simon Wright for his kind assistance in the analysis of the CHEMTAX data. This work was supported by the Helmholtz Innovation Fund Phytooptics VH-NG-300 and DFG in the framework of the priority programme "Antarctic Research with comparative investigations in Arctic ice areas" by a Grant HO 4680/1.

References

Alderkamp, A.C., de Baar, H.J.W., Visser, R.J.W., Arrigo, K.R., 2010. Can photoinhibition control phytoplankton abundance in deeply mixed water columns of the southern ocean? Limnol. Oceanogr. 55, 1248–1264.

Alderkamp, A.C., Kulk, G., Buma, A.G.J., Visser, R.J.W., Van Dijken, G.L., Mills, M.M., Arrigo, K.R., 2012. The effect of iron limitation on the photophysiology of *Phaeocystis antarctica* (Prymnesiophyceae) and *Fragilariopsis cylindrus* (Bacillariophyceae) under dynamic irradiance. J. Phycol. 48, 45–59. http://dx.doi.org/10.1111/j.1529-8817.2011.01098.x.

Arrigo, K., Ditullio, G., Dunbar, R., Robinson, D., Vanwoert, M., Worthen, D., Lizotte, M., 2000. Phytoplankton taxonomic variability in nutrient utilization and primary production in the ross sea. J. Geophys. Res. 105, 8827–8845. http://dx.doi.org/10.1029/1998JC000289.

de Baar, H.J.W., Boyd, P.W., Coale, K.H., Landry, M.R., Tsuda, A., Assmy, P., Bakker, D.C. E., Bozec, Y., Barber, R.T., Brzezinski, M.A., Buesseler, K.O., Boyè, M., Croot, P.L., Gervais, F., Gorbunov, M.Y., Harrison, P.J., Hiscock, W.T., Laan, P., Lancelot, C., Law, C.S., Levasseur, M., Marchetti, A., Millero, F.J., Nishioka, J., Nojiri, Y., van Oijen, T., Riebesell, U., Rijkenberg, M.J.A., Saito, H., Takeda, S., Timmermans, K.R., Veldhuis, M.J.W., Waite, A.M., Wong, C.S., 2005. Synthesis of iron fertilization experiments: from the iron age in the age of enlightenment. J. Geophys. Res. 110, C09S16. http://dx.doi.org/10.1029/2004JC002601.

Banse, K., 1996. Low seasonality of low concentrations of surface chlorophyll in the subantarctic water ring: underwater irradiance, iron, or grazing?. Prog. Oceanogr. 37, 241–291. http://dx.doi.org/10.1016/S0079-6611(96)00006-7.

Barlow, R., Cummings, D., Gibb, S., 1997. Improved resolution of mono-and divinyl chlorophylls a and b and zeaxanthin and lutein in phytoplankton extracts using reverse phase C-8 HPLC. Mar. Ecol. Prog. Ser. 161, 303–307.

Bowie, A.R., Griffiths, F.B., Dehairs, F., Trull, T.W., 2011. Oceanography of the subantarctic and Polar Frontal Zones south of Australia during summer: setting for the saz-sense study. Deep-Sea Res. II 58, 2059–2070. http://dx.doi.org/10.1016/j.dsr2.2011.05.033.

Boyd, P.W., 2002. Environmental factors controlling phytoplankton processes in the Southern Ocean. J. Phycol. 38, 844–861. http://dx.doi.org/10.1046/j.1529-8817.2002.t01-1-01203.x.

Boyd, P.W., Jickells, T., Law, C.S., Blain, S., Boyle, E.A., Buesseler, K.O., Coale, K.H., Cullen, J.J., de Baar, H.J.W., Follows, M., Harvey, M., Lancelot, C., Levasseur, M., Owens, N.P.J., Pollard, R., Rivkin, R.B., Sarmiento, J., Schoemann, V., Smetacek, V., Takeda, S., Tsuda, A., Turner, S., Watson, A.J., 2007. Mesoscale iron enrichment experiments 1993–2005: synthesis and future directions. Science 315, 612–617. http://dx.doi.org/10.1126/science.1131669.

Brunet, C., Lavaud, J., 2010. Can the xanthophyll cycle help extract the essence of the microalgal functional response to a variable light environment? J. Plankton Res. 32, 1609–1617. http://dx.doi.org/10.1093/plankt/fbq104.

Cheah, W., Mcminn, A., Griffiths, F.B., Westwood, K.J., Wright, S.W., Clementson, L. A., 2013. Response of phytoplankton photophysiology to varying environmental conditions in the Sub-Antarctic and Polar Frontal Zone. PLoS One 8, e72165. http://dx.doi.org/10.1371/journal.pone.0072165.

Clementson, L., Parslow, J., Turnbull, A., McKenzie, D., Rathbone, C., 2001. Optical properties of waters in the Australasian sector of the Southern Ocean. J. Geophys. Res. 106, 31611–31625. http://dx.doi.org/10.1029/2000JC000359.

Falkowski, P.G., La Roche, J., 1991. Acclimation to spectral irradiance in algae. J. Phycol. 27, 8–14. http://dx.doi.org/10.1111/j.0022-3646.1991.00008.x.

Franck, V.M., Brzezinski, M.A., Coale, K.H., Nelson, D.M., 2000. Iron and silicic acid concentrations regulate si uptake north and south of the polar frontal zone in the pacific sector of the southern ocean. Deep-Sea Res. II 47, 3315–3338. http://dx.doi.org/10.1016/S0967-0645(00)00070-9.

Goss, R., Jakob, T., 2010. Regulation and function of xanthophyll cycle-dependent photoprotection in algae. Photosynth. Res. 106, 103–122. http://dx.doi.org/10.1007/s11120-010-9536-x.

Greene, R.M., Geider, R.J., Kolber, Z., Falkowski, P.G., 1992. Iron-induced changes in light harvesting and photochemical energy conversion processes in eukaryotic marine algae. Plant Physiol. 100, 565–575. http://dx.doi.org/10.1104/pp.100.2.565.

Please cite this article as: Cheah, W., et al., Importance of deep mixing and silicic acid in regulating phytoplankton biomass and community in the iron-limited.... Deep-Sea Res. II (2016), http://dx.doi.org/10.1016/j.dsr2.2016.05.019

Hauck, J., Völker, C., Wang, T., Hoppema, M., Losch, M., Wolf-Gladrow, D.A., 2013. Seasonally different carbon flux changes in the Southern Ocean in response to the southern annular mode. Glob. Biogeochem. Cycles 27, 1236–1245. http://dx.doi.org/10.1002/2013GB004600.

Higgins, H.W., Wright, S.W., Schlüter, L., 2011. Quantitative interpretation of chemotaxonomic pigment data. In: Roy, S., Egeland, E.S., Johnsen, G., Llewellyn, C.A. (Eds.), Phytoplankton Pigments: Characterization, chemotaxonomy and applications in oceanography. Cambridge University Press, Cambridge, pp. 257–313 (Chapter 6).

Hiscock, M., Marra, J., Smith, W., Goericke, R., Measures, C., Vink, S., Olson, R., Sosik, H., Barber, R., 2003. Primary productivity and its regulation in the Pacific Sector of the Southern Ocean. Deep-Sea Res. II 50, 533–558. http://dx.doi.org/10.1016/S0967-0645(02)00583-0.

Hoppe C., Klaas C., Ossebaar S., Soppa M., Cheah W., Laglera L., Santos-Echeandia J., Rost B., Wolf-Gladrow D., Bracher A., Hoppema M., Strass V. and Trimborn S., Controls of primary production in two phytoplankton blooms in the Antarctic Circumpolar Current, Deep-Sea Res. II 2015 this issue, http://dx.doi.org/10.1016/j.dsr2.2015.10.005.

Hutchins, D.A., Sedwick, P.N., DiTullio, G.R., Boyd, P.W., Queguiner, B., Griffiths, F.B., Crossley, C., 2001. Control of phytoplankton growth by iron and silicic acid availability in the subantarctic Southern Ocean: experimental results from the saz project. J. Geophys. Res. 106, 31559–31572. http://dx.doi.org/10.1029/2000JC000333.

Khatiwala, S., Primeau, F., Hall, T., 2009. Reconstruction of the history of anthropogenic CO_2 concentrations in the ocean. Nature 462, 346–349. http://dx.doi.org/10.1038/nature08526.

Khatiwala, S., Tanhua, T., Mikaloff Fletcher, S., Gerber, M., Doney, S.C., Graven, H.D., Gruber, N., McKinley, G.A., Murata, A., Ríos, A.F., Sabine, C.L., 2013. Global ocean storage of anthropogenic carbon. Biogeosciences 10P, 2169–2191. http://dx.doi.org/10.5194/bg-10-2169-2013.

Kolber, Z., Falkowski, P.G., 1993. Use of active fluorescence to estimate phytoplankton photosynthesis in situ. Limnol. Oceanogr. 38, 1646–1665.

Kolber, Z.S., Barber, R.T., Coale, K.H., Fitzwater, S.E., Greene, R.M., Johnson, K.S., Lindley, S., Falkowski, P.G., 1994. Iron limitation of phytoplankton photosynthesis in the equatorial pacific ocean. Nature 371, 145–149. http://dx.doi.org/10.1038/371145a0.

Kolber, Z.S., Prasil, O., Falkowski, P.G., 1998. Measurements of variable chlorophyll fluorescence using fast repetition rate techniques: defining methodology and experimental protocols. Biochim. Biophys. Acta 1367, 88–106. http://dx.doi.org/10.1016/S0005-2728(98)00135-2.

Kropuenske, L.R., Mills, M.M., van Dijken, G.L., Alderkamp, A.C., Berg, G.M., Robinson, D.H., Welschmeyer, N.A., Arrigo, K.R., 2010. Strategies and rates of photoacclimation in two major Southern Ocean phytoplankton taxa: *Phaeocystis antarctica* (haptophyta) and *Fragilariopsis cylindrus* (bacillariophyceae). J. Phycol. 46, 1138–1151. http://dx.doi.org/10.1111/j.1529-8817.2010.00922.x.

Laglera, L.M., Santos-Echeandía, J., Caprara, S., Monticelli, D., 2013. Quantification of iron in seawater at the low picomolar range based on optimization of bromate/ammonia/dihydroxynaphtalene system by catalytic adsorptive cathodic stripping voltammetry. Anal. Chem. 85, 2486–2492. http://dx.doi.org/10.1021/ac303621q.

Landschützer, P., Gruber, N., Haumann, F.A., Rödenbeck, C, Bakker, D.C.E., van Heuven, S., Hoppema, M., Metzl, N., Sweeney, C., Takahashi, T., Tilbrook, B., Wanninkhof, R, 2015. The reinvigoration of the Southern Ocean carbon sink. Science 349, 1221–1224. http://dx.doi.org/10.1126/science.aab2620.

Louda, J.W., Li, J., Liu, L., Winfree, M.N., Baker, E.W., 1998. Chlorophyll-a degradation during cellular senescence and death. Org. Geochem. 29, 1233–1251. http://dx.doi.org/10.1016/S0146-6380(98)00186-7.

Mackey, M.D., Mackey, D.J., Higgins, H.W., Wright, S.W., 1996. CHEMTAX—a program for estimating class abundances from chemical markers: application to HPLC measurements of phytoplankton. Mar. Ecol. Prog. Ser. 144, 265–283. http://dx.doi.org/10.3354/meps144265.

McKew, B.A., Davey, P., Finch, S.J., Hopkins, J., Lefebvre, S.C., Metodiev, M.V., Oxborough, K., Raines, C.A., Lawson, T., Geider, R.J., 2013. The trade-off between the light-harvesting and photoprotective functions of fucoxanthin-chlorophyll proteins dominates light acclimation in *Emiliania huxleyi* (clone CCMP 1516). New Phytol. 200, 74–85. http://dx.doi.org/10.1111/nph.12373.

Moore, C.M., Seeyave, S., Hickman, A.E., Allen, J.T., Lucas, M.I., Planquette, H., Pollard, R.T., Poulton, A.J., 2007. Iron-light interactions during the crozet natural iron bloom and export experiment (crozex) I: phytoplankton growth and photophysiology. Deep-Sea Res. II 54, 2045–2065. http://dx.doi.org/10.1016/j.dsr2.2007.06.011.

Moore, C.M., Suggett, D.J., Hickman, A.E., Kim, Y.N., Tweddle, J.F., Sharples, J., Geider, R.J., Holligan, P.M., 2006. Phytoplankton photoacclimation and photoadaptation in response to environmental gradients in a shelf sea. Limnol. Oceanogr. 51, 936–949. http://dx.doi.org/10.4319/lo.2006.51.2.0936.

Morel, A., Maritorena, S., 2001. Bio-optical properties of oceanic waters: a reappraisal. J. Geophys. Res. 106, 7163–7180. http://dx.doi.org/10.1029/2000JC000319.

Morrison, A.K., Frölicher, T.L., Sarmiento, J.L., 2015. Upwelling in the southern ocean. Phys. Today, 27–32.

OC-CCI, 2015. Ocean Colour Climate Change Initiative (OC-CCI) – Phase Two – Product User Guide. 2.0.5 ed. Plymouth Marine Laboratory.

Olaizola, M., Roche, J., Kolber, Z., Falkowski, P.G., 1994. Non-photochemical fluorescence quenching and the diadinoxanthin cycle in a marine diatom. Photosynth. Res. 41, 357–370. http://dx.doi.org/10.1007/BF00019413.

Pearce, I., Davidson, A.T., Thomson, P.G., Wright, S., van den Enden, R., 2011. Marine microbial ecology in the sub-Antarctic Zone: rates of bacterial and phytoplankton growth and grazing by heterotrophic protists. Deep-Sea Res. II 58, 2248–2259. http://dx.doi.org/10.1016/j.dsr2.2011.05.030.

van de Poll, W.H., Janknegt, P.J., van Leeuwe, M.A., Visser, R.J.W., Buma, A.G.J., 2009. Excessive irradiance and antioxidant responses of an antarctic marine diatom exposed to iron limitation and to dynamic irradiance. J. Photochem. Photobiol. B 94, 32–37. http://dx.doi.org/10.1016/j.jphotobiol.2008.09.003.

van de Poll, W.H., Visser, R.J.W., Buma, A.G.J., 2007. Acclimation to a dynamic irradiance regime changes excessive irradiance sensitivity of *Emiliania huxleyi* and *Thalassiosira weissflogii*. Limnol. Oceanogr. 52, 1430–1438. http://dx.doi.org/10.4319/lo.2007.52.4.1430.

Puigcorbé, V., Roca-Martí, M., Masqué, P., Benitez-Nelson, C., van der Loeff, M.R., Laglera, L.M., Bracher, A., Cheah, W., Strass, V., Hoppema, M., Santos-Echeandía, J., Klaas, C., Particulate organic carbon export across the Antarctic Circumpolar Current at 10°E: Differences between north and south of the Antarctic Polar Front. Deep-Sea Res. II, this issue, http://dx.doi.org/10.1016/j.dsr2.2016.05.016.

R Core Team, 2014. R: A Language and Environment for Statistical Computing. R Foundation for Statistical Computing, Vienna, Austria.

Rintoul, S.R., Trull, T.W., 2001. Seasonal evolution of the mixed layer in the Subantarctic Zone south of Australia. J. Geophys. Res. 106, 31447–31462. http://dx.doi.org/10.1029/2000jc000329.

Sabine, C.L., Feely, R.A., Gruber, N., Key, R.M., Lee, K., Bullister, J.L., Wanninkhof, R., Wong, C.S., Wallace, D.W.R., Tilbrook, B., Millero, F.J., Peng, T.H., Kozyr, A., Ono, T., Rios, A.F., 2004. The oceanic sink for anthropogenic CO_2. Science 305, 367–371. http://dx.doi.org/10.1126/science.1097403.

de Salas, M.F., Eriksen, R., Davidson, A.T., Wright, S.W., 2011. Protistan communities in the Australian sector of the Sub-Antarctic Zone during SAZ-Sense. Deep-Sea Res. II 58, 2135–2149. http://dx.doi.org/10.1016/j.dsr2.2011.05.032.

Smith, R.C., Booth, C.R., Star, J.L., 1984. Oceanographic biooptical profiling system. Appl. Opt. 23, 2791–2797. http://dx.doi.org/10.1364/AO.23.002791.

Soppa, M., Dinter, T., Taylor, B., Bracher, A., 2013. Satellite derived euphotic depth in the southern ocean: implications for primary production modelling. Remote Sens. Environ. 137, 198–211. http://dx.doi.org/10.1016/j.rse.2013.06.017.

Soppa, M.A., Hirata, T., Silva, B., Dinter, T., Peeken, I., Wiegmann, S., Bracher, A., 2014. Global retrieval of diatom abundance based on phytoplankton pigments and satellite data. Remote Sens. 6, 10089–10106. http://dx.doi.org/10.3390/rs61010089.

Stramski, D., Reynolds, R.A., Babin, M., Kaczmarek, S., Lewis, M.R., Röttgers, R., Sciandra, A., Stramska, M., Twardowski, M.S., Franz, B.A., Claustre, H., 2008. Relationships between the surface concentration of particulate organic carbon and optical properties in the eastern south pacific and eastern atlantic oceans. Biogeosciences 5, 171–201. http://dx.doi.org/10.5194/bg-5-171-2008.

Strass, V., 1990. On the calibration of large-scale fluorometric chlorophyll measurements from towed undulating vehicles. Deep-Sea Res. Part A 37, 525–540. http://dx.doi.org/10.1016/0198-0149(90)90023-O.

Strass, V., Leach, H., Prandke, H., Donnelly, M., Bracher, A., Wolf-Gladrow, D. The physical environmental conditions for biogeochemical differences along the Antarctic Circumpolar Current in the Atlantic Sector during late austral summer. Deep-Sea Res. II, this issue, http://dx.doi.org/10.1016/j.dsr2.2016.05.018.

Strzepek, R.F., Harrison, P.J., 2004. Photosynthetic architecture differs in coastal and oceanic diatoms. Nature 431, 689–692. http://dx.doi.org/10.1038/nature02954.

Suggett, D.J., Moore, C.M., Hickman, A.E., Geider, R.G., 2009. Interpretation of fast repetition rate (FRR) fluorescence: signatures of phytoplankton community structure versus physiological state. Mar. Ecol. Prog. Ser. 376, 1–9. http://dx.doi.org/10.3354/meps07830.

Suggett, D.J., Moore, C.M., Marañón, E., Omachi, C., Varela, R.A., Holligan, J., 2006. Photosynthetic electron turnover in the tropical and subtropical Atlantic Ocean. Deep-Sea Res. II 53, 1573–1592. http://dx.doi.org/10.1016/j.dsr2.2006.05.014.

Sunda, W.G., Huntsman, S.A., 1997. Interrelated influence of iron, light and cell size on marine phytoplankton growth. Nature 390, 389–392. http://dx.doi.org/10.1038/37093.

Taylor, B.B., Torrecilla, E., Bernhardt, A., Taylor, M.H., Peeken, I., Röttgers, R., Piera, J., Bracher, A., 2011. Bio-optical provinces in the eastern Atlantic Ocean and their biogeographical relevance. Biogeosciences 8, 3609–3629. http://dx.doi.org/10.5194/bg-8-3609-2011.

Uitz, J., Claustre, H., Griffiths, F.B., Ras, J., Garcia, N., Sandronie, V., 2009. A phytoplankton class-specific primary production model applied to the kerguelen islands region (southern ocean). Deep-Sea Res. I 56, 541–560. http://dx.doi.org/10.1016/j.dsr.2008.11.006.

Uitz, J., Huot, Y., Bruyant, F., Babin, M., Claustre, H., 2008. Relating phytoplankton photophysiological properties to community structure on large scales. Limnol. Oceanogr. 53, 614–630. http://dx.doi.org/10.4319/lo.2008.53.2.0614.

Westwood, K.J., Griffiths, F.B., Webb, J.P., Wright, S.W., 2011. Primary production in the sub-antarctic and polar frontal zones south of Tasmania, Australia; SAZ-Sense survey, 2007. Deep-Sea Res. II 58, 2162–2178. http://dx.doi.org/10.1016/j.dsr2.2011.05.017.

Wright, S.W., van den Enden, R.L., Pearce, I., Davidson, A.T., Scott, F.J., Westwood, K. J., 2010. Phytoplankton community structure and stocks in the Southern Ocean (30–80°E) determined by CHEMTAX analysis of HPLC pigment signatures. Deep-Sea Res. II 57, 758–778. http://dx.doi.org/10.1016/j.dsr2.2009.06.015.

Please cite this article as: Cheah, W., et al., Importance of deep mixing and silicic acid in regulating phytoplankton biomass and community in the iron-limited.... Deep-Sea Res. II (2016), http://dx.doi.org/10.1016/j.dsr2.2016.05.019